Synthesis, X-ray Diffraction Characterization, and Radiative Properties of $Er_2O_3-ZrO_2$ Nanocrystals Embedded in LAS Glass Ceramic

Pietro Riello,*,† Stefania Bucella,† Radenka Krsmanovic,† Stefano Meneghetti,† Serena Pietrantoni,‡ and Roberto Francini‡

Dipartimento di Chimica Fisica, Università di Venezia Ca' Foscari, Via Torino 155b, 30170 Venezia-Mestre, Italy, and Dipartimento di Fisica and Istituto Nazionale di Fisica della Materia, Università di Roma Tor Vergata, Via della Ricerca Scientifica 1, 00133 Roma, Italy

Received: February 22, 2005; In Final Form: May 6, 2005

Low thermal expansion $Li_2O-Al_2O_3-SiO_2$ (LAS) glass ceramic was examined as a host matrix for erbium ions. ZrO_2 was added to the glass since it serves as a nucleating agent and as a good environment for the luminescent ions. The study was carried out on amorphous powders of the $Li_2O-Al_2O_3-SiO_2/ZrO_2/Er_2O_3$ system prepared by the sol−gel method and successively crystallized at different temperatures. X-ray diffraction (XRD), transmission electron microscopy (TEM), and infrared (IR) spectroscopy were employed to study the evolution of the crystalline phases and the distribution of the erbium ions. The TEM micrographs confirmed that, after thermal treatment at 1000 °C, the crystallization of nanoparticles constituted by an $Er_2O_3-ZrO_2$ solid solution with narrow size distribution could be achieved. On the contrary, erbium silicate was detected in the samples without ZrO_2. The repartition constant of Er_2O_3 between ZrO_2 and LAS matrix has been also evaluated.

1. Introduction

Transparent glass ceramics containing nanosized crystalline phases doped with luminescent lanthanide elements find applications as solar collectors, up-conversion devices, and laser active and passive media.[1−6] With these materials, one can hope to put together the best properties of glass and crystals in order to obtain crystal-like optical properties in a composite characterized by the macroscopic properties of the glass, such as transparency and optical isotropy. Thus, depending on the glass host and crystal phase composition, it is possible to obtain materials with improved mechanical, thermal, electrical, and/or optical properties. Moreover, this approach seems to be very interesting, especially if the rare-earth-doped crystals are difficult to grow as single crystal because of their high melting point.[7,8]

Particular attention has been devoted to fluoride glasses that combine optical transparency and low nonradiative relaxation. Unfortunately, these materials have less favorable chemical and mechanical properties compared to oxide glasses. Aluminosilicate glass ceramics containing Er^{3+}- and Yb^{3+}-doped cubic fluoride nanocrystalline phases have indicated the possibility to follow an alternative approach that combines the benefits of the silica-based glass with a suitable local environment for the rare earth ions.[9] An important requirement is that the crystallite size should be sufficiently small to keep Rayleigh scattering losses as low as possible.

Some recent studies show that zirconium oxide is an excellent material for optical application due to its optical transparency, hardness, high chemical and photochemical stability, high refractive index and, very important, its low phonon energy.[9−11] This fact suggests the possibility of obtaining Er^{3+}/ZrO2 nanocrystals embedded in a glass or a glass-ceramic matrix.

In the present work, we explore the possibility of developing luminescent oxide glass ceramics in the LAS system characterized by high thermal and mechanical strength and transparency.[12] This group of glass ceramics is usually nucleated with ZrO_2, TiO_2, P_2O_5 or with a combination of two or more of them.[13,14] In this way, a large number of nanocrystallites (5−20 nm), belonging to the nucleating phase (for example ZrO_2 or $ZrTiO_4$), develop in the glassy matrix. Some recent studies deal with the luminescent properties of Er-doped ZrO_2 and TiO_2 nanocrystals[10,11,15] or with glasses where the erbium-containing nanocrystals ($Er_2Ti_2O_7$, $ErPO_4$)[16−18] develop after thermal treatments.

Only few studies concern luminescent materials based on the LAS system.[5,6] These studies show that even if the Nd^{3+}-doped glass is nucleated using ZrO_2, the rare earth ions seem to be located inside the silica-rich phases.

As mentioned above, it is fundamental to control the local environment of the Er^{3+} ions, both to reduce dissipative processes and to limit the concentration level of the rare earth known to cause a reduction of the luminescence intensity.[19] One serious problem that faced us, in fact, involved the clustering of the erbium ions into the demixed crystalline phases: if on one hand it is better to remove the active ions from the high phonon frequency silica matrix, on the other hand this results in segregation which especially, in particular for the Er^{3+}, leads to concentration quenching.

In the present work we analyze the distribution of Er^{3+} ions in LAS glass ceramic, and in particular we are interested in the possibility of transferring the active ions into the ZrO_2 nuclei. The difference between samples containing different amounts of zirconium oxide is taken into account.

The aim of this work is to evaluate the amount of erbium that it is possible to transfer into zirconia nanocrystals from the LAS phases matrix. The repartition constant between zirconia and the matrix is calculated from X-ray quantitative

* Corresponding author. E-mail: riellop@unive.it
† Università di Venezia Ca' Foscari.
‡ Università di Roma Tor Vergata.

10.1021/jp050919a CCC: $30.25
Published on Web 06/23/2005

analysis. This approach allows to foresee the content of zirconia added to the glass necessary to drain the desired amount of the RE from the matrix.

The erbium-doped LAS glass ceramic samples were obtained by thermal treatment of powders prepared by the sol−gel process. For the synthesis water medium and metal formate, salts of Al, Li and Zr were preferred to the alcoholic medium and expensive metal alcoxides.[20] The sol−gel route was employed because of the possibility of preparing homogeneous multicomponent hydroxidic precursors processable at lower temperatures than those required by the melting technique.

Transmission electron microscopy (TEM) was employed to determine morphology and particle size of the Er_2O_3- and ZrO_2-rich phases and, coupled with EDX analysis, their composition.

The quantitative phase analysis by X-ray diffraction was performed using the Rietveld method (DBWS9600 computer program written by Sakthivel & Young and modified by P.Riello et al.[21]). By using this procedure, it is possible to perform the quantitative analysis of the crystalline phases, even if an amorphous matrix is present, without adding any internal standard to the sample. The quantification of the different phases is possible because during the crystallization process the whole chemical composition of the sample does not change. This procedure has been usefully applied to the study of many kinds of materials and in particular to the study of crystallization of LAS glass ceramic.[14]

Finally, a photoluminescence study gave insight into the distribution of Er^{3+} ions when their concentration was too low to be detected by the XRD and EDX analysis, and also into the relative luminescence efficiencies of erbium ions in the different phases.

2. Experimental Section

2.1. Chemicals, Synthesis, and Processing. The LAS samples were prepared with the molar composition $SiO_2/Al_2O_3/Li_2O/Er_2O_3$ 1:0.18:0.10:0.005. Two different contents of zirconium oxide, corresponding to the ZrO_2/Er_2O_3 ratio of 2.7 and 11, were used. The pure LAS matrix and the samples without Er_2O_3 or ZrO_2 were also prepared. Three solid solutions, $(Er_2O_3)_x(ZrO_2)_{(1-x)}$ (with composition $x = 0.026$, 0.053, and 0.143) have been prepared by precipitation of the chloride salts with ammonia, in order to verify the relationship between cell parameter and composition of the ZrO_2 s.s. These samples were also used as a standard for the optical spectroscopy measurements.

The starting materials were tetraethoxy silane (TEOS) (98% Aldrich), lithium carbonate (99% Aldrich), zirconium oxychloride octahydrate (98% Aldrich), aluminum nitrate nonahydrate (98% Aldrich), and erbium chloride hexahydrate (99.9% Aldrich).

The LAS samples were prepared as follows: freshly prepared aluminum and zirconium hydroxides, obtained by the addition of 30% ammonia to the saltwater solutions, were reacted with formic acid; lithium formate was prepared from lithium carbonate; erbium was directly introduced as chloride salt; TEOS was in the end added to the water solution containing the right amount of metal ions. The sol was heated at 70 °C until gelation took place. The resulting powder was annealed in air for 24 h at 490, 800, 900, and 1000 °C.

In the following, the samples containing ZrO_2 are referred to as LAS−Er−$Zr_{(2.7 \text{ or } 11)}$-X, where X is the annealing temperature; the samples without ZrO_2 are referred to as LAS−Er-X, and the matrices without erbium as LAS−Zr and LAS.

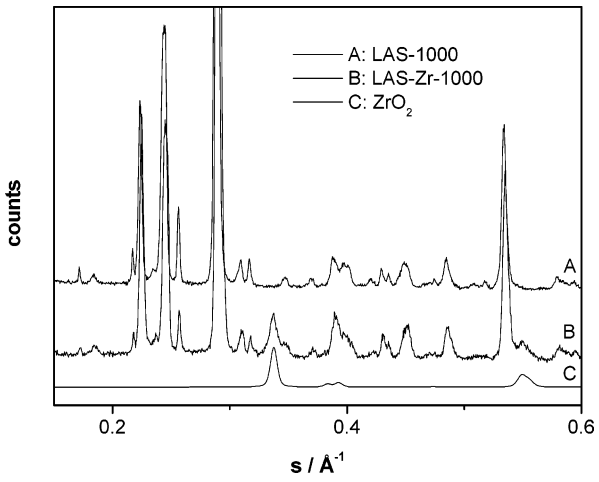

Figure 1. Comparison of the XRD patterns of LAS with and without the ZrO_2.

2.2. Physical Characterization. The XRD patterns were collected at room temperature with a step size of 0.05° in the preset-time mode (10 s). To improve the signal-to-noise ratio at least 3 runs were measured. Philips diffractometers, equipped with a focusing graphite monochromator on the diffracted beam and with a proportional counter with an electronic pulse height discrimination, were used. Moreover, a divergence slit of 0.5°, a receiving slit of 0.2 mm., an anti-scatter slit of 0.5°, and Fe-filtered CoKα and Ni-filtered CuKα radiations were employed.

Average crystallite sizes were calculated using the Scherrer's equation ($\langle d \rangle = \lambda/\beta \cos \theta$), while correction for instrumental broadening proved to be negligible.

TEM images were taken at 300 kV with a JEOL 3010 instrument with an ultrahigh resolution (UHR) pole-piece (0.17 nm point resolution), equipped with a Gatan slow-scan CCD camera (model 794) and an Oxford Instrument EDS microanalysis detector (model 6636). The powdered samples were dispersed in isopropyl alcohol solution by sonication for about five minutes and then deposited onto a holey carbon film.

For the infrared (IR) spectroscopic investigations, the powder samples were manually pressed inside a plastic washer and were held in place by two fused-silica microscope slides, one of which served both as input window for the exciting laser beam and as output window for the collection of the luminescence. All measurements were performed at room temperature by exciting the erbium ions at 980 nm using a continuos wave InGaAsP laser diode. The maximum laser power was about 1 W, but for stable operation a power of 400 mW was chosen. The laser beam was weakly focused on the sample to a spot of approximately 1 mm^2, corresponding to a power density of about 40 W/cm^2. The luminescence from the sample was collected and analyzed by a 30 cm focal length monochromator and detected with a cooled germanium detector.

3. Results

3.1. TEM and XRD Characterization. LAS matrices with and without zirconium oxide do not show significant differences concerning the main phases, apart from the presence of *t*-ZrO_2 (see Figure 1).

The details about phase composition (wt %), determined through the XRD Rietveld quantitative analysis, and average crystallite size ($\langle d \rangle$, nm) of the main phases of the Er^{3+}-doped LAS samples are summarized in Table 1. The estimated errors on the quantitative phase analysis are obtained by propagating

TABLE 1: Phase Composition and Crystallite Sizes of the LAS Treated at Different Temperature[a]

	LasErZr2.7			LasErZr11			LasEr		
T(°C)	800	900	1000	800	900	1000	800	900	1000
amorphous (wt %)	99 ± 0.2	48 ± 1	17 ± 1.5	89 ± 0.5	56 ± 1	7 ± 2	80 ± 0.5	42 ± 2	31 ± 1
$(Er_2O_3)_xZrO_{2(1-x)}$ (wt %)		2 ± 0.1	3 ± 0.1	5 ± 0.1	5 ± 0.2	8 ± 0.3			
		$x = 0.16$	$x = 0.16$	$x = 0$	$x = 0.065$	$x = 0.074$			
d (nm)		15	17	4	6.7	7.7			
$Er_2Si_2O_7$ (wt %)							<1	<1	1.3 ± 0.1
d (nm)									40
β-eucryptite (wt %)	1 ± 0.2	34 ± 0.5	45 ± 1	4 ± 0.1	26 ± 0.5	54 ± 0.1	7 ± 0.5	39 ± 1	24 ± 1
d (nm)		30	24	33	26	20	26	27	22
β−spodumene (wt %)		11 ± 0.5	27 ± 1			8 ± 1	10 ± 0.5	8 ± 1	40 ± 1
d (nm)		29	34			36	22	53	31
cristobalite (wt %)		2 ± 0.1	<1	2 ± 0.3	11 ± 1	17 ± 1	<1	2.5 ± 0.5	<1
d (nm)		29			20	21		27	
β−spodumene2 (wt %)							3 ± 0.5	8 ± 1	
d (nm)							34	34	
mullite (wt %)		3 ± 0.4	7 ± 0.7		2 ± 1	6 ± 1			3.5 ± 0.5
d (nm)		38	35		33	33			38

[a] The composition of eucryptite s.s. is derived from the cell parameters according to Nakagawa et al.[24] The relationship between the size d of a spherical nanocrystal obtained by the Sherrer equation and its diameter is $2R = 4d/3$.

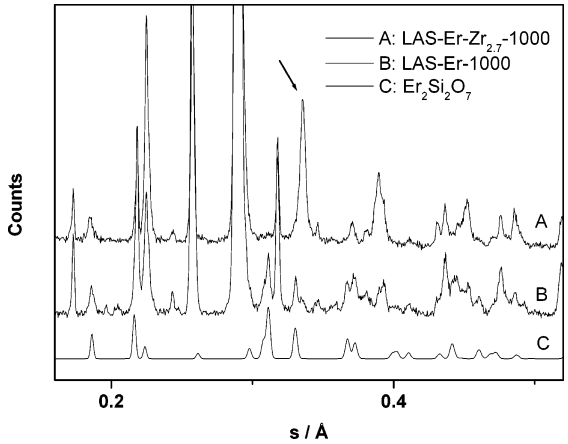

Figure 2. LAS−Er−$Zr_{2.7}$-1000 and LAS−Er-1000 XRD patterns. The arrow shows the position of the peaks belonging to the Er_2O_3−ZrO_2 s.s.

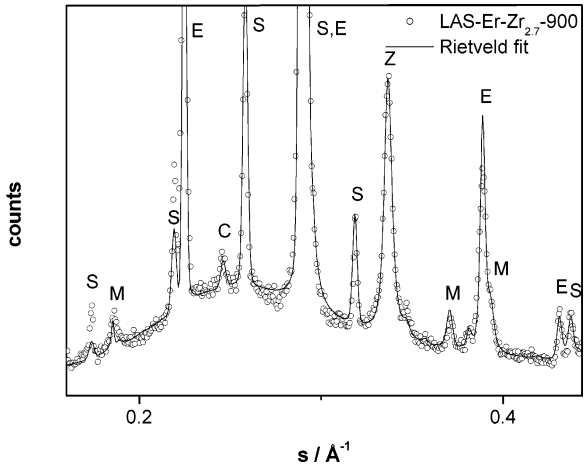

Figure 3. XRD pattern of LAS−Er−Zr2.7-900. S: β-spodumene s.s.; E: β-eucriptite s.s.; C: cristobalite; M: mullite; Z: $Er_{0.28}Zr_{0.72}O_{1.86}$.

the scale factors and cell parameter errors obtained by the Rietveld fitting procedure.

By comparing samples annealed at the same temperature (see Table 1), we observe that the most important difference is that while the main LAS phases (β-eucryptite s.s., hexagonal space group $P6_222$, and β-spodumene s.s., tetragonal space group $P4_32_12$) always remain the same, a segregation of RE into the stoichiometric compound $Er_2Si_2O_7$ (monoclinic space group C12/m1) takes place only when zirconia is not added (see Figure 2). The amount of erbium oxide crystallized as $Er_2Si_2O_7$ is evaluated to be 45% of the introduced oxide, therefore 55% remains in the amorphous or/and in the silica-rich crystalline LAS phases.

In LAS−Er-800 and -900 there are two phases that at 1000 °C cannot be clearly identified: a β-quartz s.s. (β-eucryptite s.s. very rich in SiO_2) and another phase very similar to β-spodumene (referred as β-spodumene2 in Table 1). The ratio between β−eucryptite and β−spodumene becomes smaller as the temperature increases: this behavior is typical of this kind of glasses.[6,22]

While LAS−Er−$Zr_{2.7}$ 800 °C is nearly completely amorphous, containing only 1 wt % of β-eucryptite, the analysis of the pattern of LAS−Er−$Zr_{2.7}$-900 (Figure 3) and −1000 shows that the major phases, β-eucryptite and β-spodumene s.s., are present together with small amounts of cristobalite and mullite.

TABLE 2: Percentage of the Introduced Er_2O_3 and ZrO_2 Crystallized as $(Er_2O_3)_x(ZrO_2)_{(1-x)}$

	LasEr			LasErZr2.7			LasErZr11		
T(°C)	800	900	1000	800	900	1000	800	900	1000
ZrO_2					77	95	37	57	83
Er_2O_3	<1.0	16	45		44	49		48	77

While neither erbium oxide, zirconium oxide, nor erbium silicate are detectable, a cubic Er_2O_3-stabilized ZrO_2 s.s. (space group $Fm3m$) can be ascribed to the phase having the major peak centered at 0.336 $Å^{-1}$.

To establish the composition of the latter phase we used the equations for cubic and tetragonal lattice parameters of Y_2O_3-stabilized ZrO_2:[23] $a(nm) = 0.5114+0.000283x$, $7 < x$ (mol % Y_2O_3) < 35; $a(nm) = 0.5079+0.0006x$, $c(nm) = 0.5194-0.0006X$, $3 < x$ (mol % Y_2O_3) < 8. More specifically, because of the broadness of the peaks, when the content of Er_2O_3 in the s.s. was in the range in which ZrO_2 is stabilized into the tetragonal form, the latter equations were employed considering the cell volume (V^{cell}) instead of the two lattice parameters separately.

The applicability of the above-mentioned equations is justified by the negligible difference between the Y^{3+} and the Er^{3+} radii. Additionally, we verified the legitimacy of this assumption applying the equations for cubic and tetragonal lattice parameters

TABLE 3: Cell Parameter Data and Quantitative Results for Three Standard $(Er_2O_3)_x(ZrO_2)_{(1-x)}$ Samples

x (nominal)	*x* (calculated)	monoclinic (wt %)	tetragonal (wt %)[a]	cubic (wt %)[a]
0.143	0.147			100 a=5.175
0.053	0.049		86	14
			$x = 0.045$	$x = 0.077$
			$a = 3.613$	$a = 5.133$
			$c = 5.16$	$\alpha = \beta = \gamma = 90$
			$\alpha = \beta = \gamma = 90$	
0.026	0.03	17	83	
		$a = 5.163$	$x = 0.037$	
		$b = 5.202$	$a = 3.606$ $c = 5.175$	
		$c = 5.322$	$\alpha = \beta = \gamma = 90$	
		$\alpha = 90$ $\beta = 99.2$ $\gamma = 90$		

[a] $x = Er_2O_3$ mol % in the zirconate solid solution.

of Y_2O_3-stabilized ZrO_2[23] on three Er_2O_3-doped ZrO_2 standard samples containing different amounts of stabilizer (2.5, 5, and 14 mol %). Cell parameter data and quantitative results for the three standard samples are reported in Table 3. We assumed that the monoclinic phase in the sample with the lowest amount of Er_2O_3 is pure ZrO_2.

In this way we estimated that both in LAS−Er−$Zr_{2.7}$-900 and LAS−Er−$Zr_{2.7}$-1000, the zirconate s.s. has the composition $Er_{0.28}Zr_{0.72}O_{1.86}$ (16 mol % Er_2O_3, a = 5.159 Å). From the amount of the phase obtained by the Rietveld refinement, we calculated that at 900 °C, 44 wt% of Er_2O_3 crystallizes as zirconate s.s. At 1000 °C this value increases up to 49 wt%. As in the LAS−Er samples, the remaining 56 and 51% might be inside the amorphous or/and the crystalline LAS phases. It must be said that even if the total amount of Er^{3+} were all dissolved inside the crystalline LAS phases, its concentration would be under the detection limit of the XRD analysis and, in any case, it would be impossible to ascribe the observed changes of cell parameter of β-eucryptite and β-spodumene s.s. to different amounts of Er^{3+} rather than Al^{3+}ions.[24] Only the spectroscopic characterization will clarify this point, as described below.

The composition of the $ZrO_2-Er_2O_3$ s.s. in LAS−Er−Zr_{11}-1000, calculated, as above, by the equation for cubic lattice parameters of Y_2O_3-stabilized ZrO_2, results to be $Er_{0.14}Zr_{0.86}O_{1.93}$ (7.4 mol % Er_2O_3, a = 5.135 Å) and the amount of Er_2O_3 crystallized as $ZrO_2-Er_2O_3$ s.s. is 77%.

At 900 °C a smaller amount of erbium enters into the zirconia structure in comparison with LAS−Er−$Zr_{2.7}$ annealed at the same temperature: the composition results to be $Er_{0.12}Zr_{0.88}O_{1.94}$ (6.5 mol % Er_2O_3, $V^{cell} = 67.295$), and only 43 wt % of Er_2O_3 is crystallized in this phase. At 800 °C a pure size-stabilized tetragonal zirconia develops.

TEM micrographs (Figure 4) of LAS−Er−Zr_{11}, LAS−Er−$Zr_{2.7}$, and LAS−Er, all annealed at 1000 °C, evidence that a narrower size distribution with smaller particles of the erbium rich phases is obtained when ZrO_2 is present.

The results obtained by using the equations for the lattice parameters of Y_2O_3-stabilized ZrO_2 were also confirmed by the EDX analysis (Figure 5) carried out on the nanoparticles of Figure 4. If we compare the EDX spectra of LAS−Er−Zr_{11} and LAS−Er−$Zr_{2.7}$, we observe that the Zr/Er ratio is higher in the former one. Additionally, the Er concentration in the matrix situated far from the particles is too low to be revealed by EDX analysis.

The quantitative analysis, combined with the knowledge of the size of the particles, allows the evaluation of the $Er_2O_3-ZrO_2$ nanoparticle concentration.[14] The best results were obtained with the LAS−Er−Zr_{11}-900 and LAS−Er−Zr_{11}-1000 samples where there is an erbium doped nanoparticle concentration of about 5.5×10^{16} cm^{-3}, while for the samples LAS−Er−$Zr_{2.7}$ the concentration is 1.8×10^{15} cm^{-3}. The estimated error on these concentrations is typically 10% and it mainly derives from the error on the average volume of the nanoparticles.

3.2. Optical Characterization. The optical spectroscopy study of the different LAS and erbia stabilized ZrO_2 samples was focused on the 1.5 μm infrared emission transition $^4I_{13/2} \rightarrow {}^4I_{15/2}$ connecting the first excited multiplet to the ground-state multiplet of Er^{3+}. Shining the powder samples with 980 nm light yields a population of excited Er^{3+} ions in the $^4I_{11/2}$ electronic state, which rapidly decays to the $^4I_{13/2}$ next lower excited state.

The excitation mechanism is not selective with respect to erbium ions belonging to different phases and/or different site symmetries within the same phase. As a result, the emission-

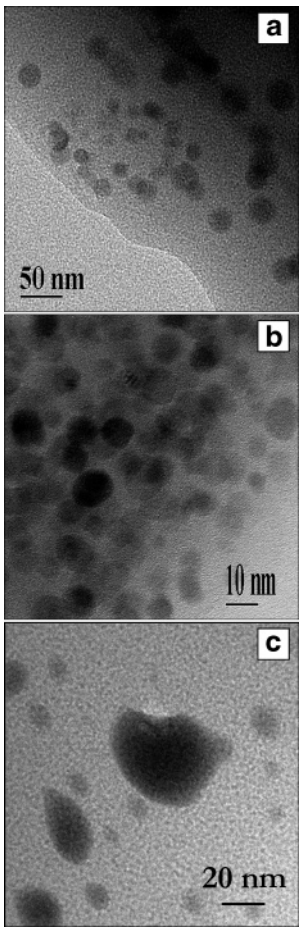

Figure 4. TEM images of (a) LAS−Er−$Zr_{2.7}$-1000; (b) LAS−Er−Zr_{11}-1000; (c) LAS−Er-1000.

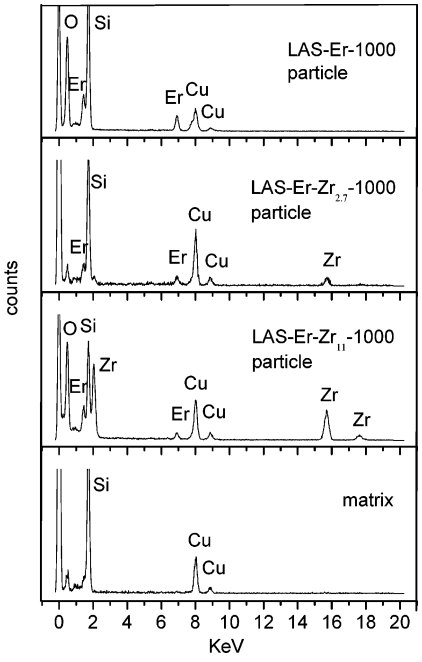

Figure 5. EDX analysis. From the top: $Er_2Si_2O_7$ (LAS−Er-1000); $Er_2O_3-ZrO_2$ s.s. (LAS−Er−$Zr_{2.7}$-1000), $Er_2O_3-ZrO_2$ s.s. (LAS−Er−Zr_{11}-1000); matrix (LAS−Er-1000).

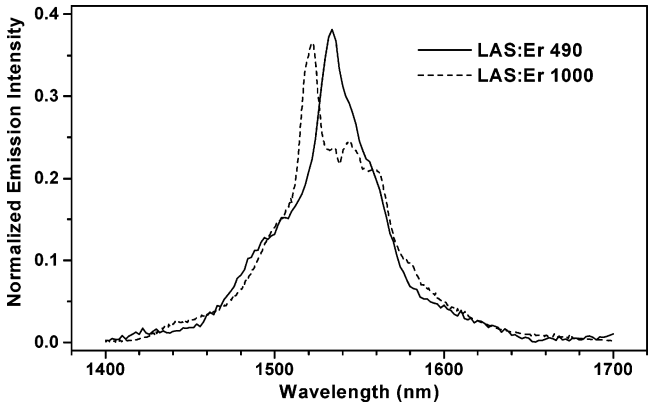

Figure 6. Room-temperature emission spectra excited at 980 nm of the LAS−Er-490 and LAS−Er-1000 samples. Each spectrum is normalized to the emission intensity integrated over the whole spectrum.

spectra line shape reflects contributions from several emitting erbium centers.

The emission spectra of the LAS−Er-490 (amorphous) and LAS−Er-1000 samples are shown in Figure 6. The erbium ions in the amorphous sample are dispersed in a disordered matrix and a broad, unstructured emission line shape, typical of erbium-doped glasses, with a single peak at 1534 nm is observed. In the LAS−Er sample annealed at the highest studied temperature (1000 °C), the integrated emission intensity is about 100 times higher than that of the amorphous sample. The emission line shape remains broad, but several structures can now be observed and the main peak shifts to 1522 nm.

From Table 1, we see that the LAS−Er-1000 sample contains several crystalline nanophases, namely, 40 wt % of β-spodumene, 24 wt % of β-eucryptite, and 1.3 wt % of $Er_2Si_2O_7$ with an erbium ion distribution of 45 wt % in the stoichiometric compound $Er_2Si_2O_7$. The observed structures in Figure 6 originate from the emission of erbium ions belonging to the various crystalline phases. Further insight about the contribution of $Er_2Si_2O_7$ to the overall luminescence emission comes from the comparison of the spectra of LAS−Er-1000 and the two

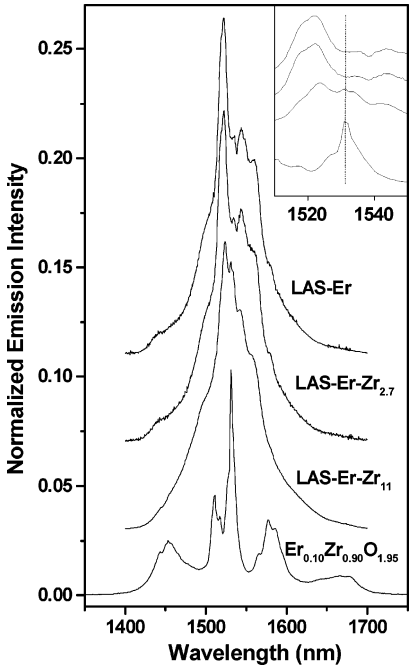

Figure 7. Room-temperature emission spectra excited at 980 nm of the LAS−Er, LAS−Er-$Z_{2.7}$, LAS−Er−Zr_{11}, and $Er_{0.10}Zr_{0.90}O_{1.95}$ samples, annealed at 1000 °C. Each spectrum is normalized to the emission intensity integrated over the whole spectrum. The inset shows the spectral region around the main peak of the erbium zirconate.

LAS−Er−Zr samples, where such a crystalline phase is absent. In Figure 7, the infrared emission spectra of all the samples annealed at 1000 °C are compared. The LAS sample with a low zirconia content (LAS−Er−$Zr_{2.7}$) has an emission line shape very similar to that of the LAS−Er-1000 sample, thus confirming that the main contributions to the infrared emission arise from the eucryptite and spodumene phases, while the erbium $^4I_{13/2} \rightarrow {}^4I_{15/2}$ transition from the $Er_2Si_2O_7$ phase cannot be detected. The zirconate phase should be observed at this stage (49 wt % of erbia crystallizes in this phase), but the oscillator strength of the $f-f$ erbium transitions is too weak to be observed under the stronger emissions from the erbium sites of eucryptite and spodumene. Significant changes in the emission line shape are observed for the LAS sample with the higher concentration of zirconia (LAS−Er−Zr_{11}), although the main features are still comparable with those of the other LAS samples. LAS−Er−Zr_{11} has the composition shown in Table 1, with 54 wt % of eucryptite, 8 wt % of spodumene, and a concentration of 8 wt % of erbium zirconate, approximately three times that of LAS−Er−$Zr_{2.7}$, with 77% of erbia crystallized in the latter phase. It is worth noticing that (see the inset of Figure 7) a very small structure appears at 1531 nm, corresponding to the main peak of the $^4I_{13/2} \rightarrow {}^4I_{15/2}$ Er^{3+} transition in the emission spectrum of the erbia-stabilized zirconia $(Er_2O_3)_{0.053}(ZrO_2)_{0.947}$ sample (Figure 7).

Last, considering that the amount of the amorphous phase in LAS−Er, LAS−Er−$Zr_{2.7}$, and LAS−Er−Zr_{11} is 31, 17, and 7 wt %, respectively, and that the emission line shapes, apart from the small structure corresponding to the zirconate s.s. mentioned above, are very similar, we can state that the erbium emission belongs to the aluminosilicate phases.

4. Discussion

4.1. Microstructure. As shown in Table 1, in the LAS−Er and LAS−Er−$Zr_{2.7}$ samples annealed at 1000 °C about half of the introduced erbium oxide is subject to segregation, developing

a silicate ($Er_2Si_2O_7$) and a zirconate ($Er_xZr_{1-x}O_{2-x/2}$) phase, respectively. Consequently, a large amount of erbium is lost because of a strong concentration quenching mechanism. However, there is a very important difference between the formation of the two phases. In fact, the composition of the erbium silicate phase cannot be changed because it is a stoichiometric compound, while in the erbium zirconate phase, which is a solid solution, the concentration of the luminescence ions may be changed.

The LAS−Er−Zr and LAS−Er samples differ also in particle size and size distribution of the erbium rich phases: $Er_2Si_2O_7$ particles are always bigger and have a broader size distribution in comparison to zirconate ones (see Figure 4c).

It is interesting to observe that the composition of the $Er_2O_3-ZrO_2$ s.s. in LAS−Er−$Zr_{2.7}$-1000 compared with that developed in LAS−Er−$Zr_{2.7}$-900 has not changed and that only the increase of crystallinity implies that a higher amount of Er_2O_3 crystallizes as solid solution.

Even if these two samples evidence the important result obtained by the addition of ZrO_2, they also evidence that the amount of this phase in LAS−Er−$Zr_{2.7}$ proved to be inadequate in draining most of the RE from the silica-rich matrix into the more favorable zirconate phase. Because of this, samples with a larger amount of zirconia, LAS−Er−Zr_{11}, were prepared. Also, the dilution of the RE into the ZrO_2 phase was expected to improve luminescence efficiency.

The quantitative results obtained by the Rietveld refinement on LAS−Er−$Zr_{2.7}$ and LAS−Er−Zr_{11} samples treated at 1000 °C (see Table 2 for the percentage of the introduced Er_2O_3 and ZrO_2 crystallized as $(Er_2O_3)_x(ZrO_2)_{(1-x)}$) allowed us to state that the partition constant of Er_2O_3 between ZrO_2 and the matrix ($K = [Er_2O_3]_{ZrO}2/[Er_2O_3]_{matrix}$) is about 90. With this value it is possible to foresee that in order to drain the 95% of Er_2O_3 into ZrO_2, the content of the latter phase should be 24 mol % and the composition of the resulting solid solution would be $(Er_2O_3)_{0.02}(ZrO_2)_{0.98}$.

The particle size (volume weighted) of the LAS−Er−Zr samples obtained by the Scherrer equation corresponds to the one obtained by TEM analysis, indicating the single domain of the particles and the narrowness of the distribution. As described in the results section, a very high concentration of nanoparticles (5.5×10^{16} cm^{-3}) was obtained in LAS−Er−Zr_{11}-1000.

4.2. Luminescence. Both the line shape and the infrared luminescence efficiency of erbium ions are sensitive to the structure in which zirconia is forced by the nanometric dimensions and the stabilizing action of erbia.[25] The local structure of erbium ions is responsible for the amount of splitting of the 4f-multiplets as well as for the number of Stark components.

The erbia-stabilized zirconia nanocrystals are rich in oxygen vacancies which can be localized in the nearest neighbor shell of the Er^{3+} ions. Thus, a fraction of erbium sites deviate from the otherwise tetragonal or cubic symmetry, resulting in a complex emission line shape made of mostly unresolved contributions from the different sites.[26,27]

In the investigated LAS−Er−Zr samples, the fraction of erbia segregated in phases other than zirconia is sufficiently large enough to induce an IR luminescence of intensity that is comparable to or even larger than that of erbium zirconate contained in the same sample. These results suggest that, although a significant improvement is achieved with a Zr/Er ratio of 11, one should further increase this ratio in order to maximize the fraction of erbia that crystallizes in the zirconia nanoparticles. Moreover, a higher Zr/Er ratio is beneficial as results in a net reduction of the erbium concentration in the ZrO_2 phase. The requirement of a lower Er^{3+} concentration can be understood by comparing the integrated IR emission intensities of the three erbia-stabilized zirconia standard samples, as shown in Figure 8. We can see that for Er_2O_3 concentrations higher than 5.3 mol %, the emission intensity is significantly reduced due to erbium−erbium interaction. This concentration quenching mechanism is a well-known effect that imposes an upper limit to the amount of erbium ions in view of the possible optical applications of these materials.

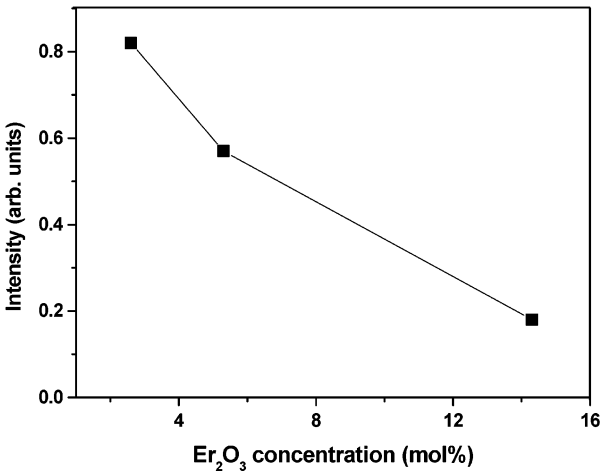

Figure 8. Integrated emission intensities at 1.5 μm vs molar concentration of erbia for the three ZrO_2 samples stabilized with different amount of Er_2O_3: 2.6, 5.3, and 14.3 mol %.

5. Conclusions

To study the phase compositions and to evaluate the repartition constant of Er_2O_3 between the ZrO_2 and LAS matrix, several samples were prepared by sol−gel techniques. In this way erbium-doped zirconia nanoparticles embedded in a $Li_2O-Al_2O_3-SiO_2$ glass ceramic have been successfully prepared using the aqueous sol−gel method that allows more feasible conditions than those required by melting. The combined use of optical infrared spectroscopic, TEM, and XRD analysis allowed us to determine the distribution of erbium ions among the different phases.

Even if the amounts of lanthanide used in the preparation of the samples was high in view of a possible optical application, because of the concentration quenching mechanism, we found that ZrO_2 behaves as a very good solvent, extracting most of the rare earth from the silica-rich matrix and draining it into the more favorable zirconia environment. The repartition constant of Er_2O_3 between ZrO_2 and the LAS matrix was 90 at 1000 °C. In particular, we observed that by adding different contents of zirconium oxide and with controlled thermal treatments, it is possible to regulate the amount, the composition, and the size of the $Er_2O_3-ZrO_2$ s.s. nanoparticles.

Acknowledgment. Financial support from MURST (PRIN-2002) and INFM is gratefully acknowledged.

References and Notes

(1) Malyarevich, A. M.; Denisov, I. A.; Volk, Y. V.; Yumashev, K. V.; Dymshits, O. S.; Zhilin, A. A. *J. Alloys Compd.* **2002**, *341*, 247.

(2) Auzel, F.; Lipinska-Kalita, K. E.; Santa-Cruz, P. *Opt. Mater.* **1996**, *5*, 75.

(3) Mortier, M.; Auzel, F. *J. Non-Cryst. Solids* **1999**, *256*−*257*, 361.

(4) Mortier, M.; Monteville, A.; Patriarche, G.; Mazé, G.; Auzel, F. *Opt. Mater.* **2001**, *16*, 255.

(5) Dymnikov, A. A.; Dymshits, O. S.; Zhilin, A. A.; Savostjanov, V. A.; Chuvaeva, T. I. *J. Non-Cryst. Solids* **1996**, *196*, 67.
(6) Kang, U.; Chuvaeva, T. I.; Onushchenko, A. A.; Shashkin, A. V.; Zhilin, A. A.; Kim, H.-J.; Chang, Y.-G. *J. Non-Cryst. Solids* **2000**, *278*, 75.
(7) Vivien, D. *Ann. Chim. Sci. Mat.* **2003**, *28*, 1.
(8) Mortier, M. *Ann. Chim. Sci. Mat.* **2003**, *28*, 21.
(9) Wang, Y.; Ohwaki, J. *Appl. Phys. Lett.* **1993**, *63*, 3268.
(10) De la Rosa-Cruz, E.; Diaz-Torres, L. A.; Rodriguez-Rojas, R. A.; Meneses-Nava, M. A.; Barbosa-Garcia, O. *Appl. Phys. Lett.* **2003**, *83*, 4903.
(11) Patra, A.; Friend, C. S.; Kapoor, R.; Prasad, P. N. *J. Phys. Chem. B* **2003**, *83*, 284.
(12) Guedes, M.; Ferro, A. C.; Ferreira, J. M. F. *J. Eur. Ceram. Soc.* **2001**, *21*, 1187.
(13) Lin, M.-H.; Wang, M.-C. *J. Mater. Res.* **1996**, *11*, 2611.
(14) Riello, P.; Canton, P.; Comelato, N.; Polizzi, S.; Verità, M.; Fagherazzi, G.; Hofmeister, H.; Hopfe, S. *J. Non-Cryst. Solids* **2001**, *288*, 127.
(15) Jeon, S.; Braun, P. V. *Chem. Mater.* **2003**, *15*, 1256.
(16) Coutier, C.; Meffre, W.; Jenouvrier, P.; Fick, J.; Audier, M.; Rimet, R.; Jacquier, B.; Langlet, M. *Thin Solid Films* **2001**, *392*, 40.
(17) Coutier, C.; Audier, M.; Fick, J.; Meffre, W.; Rimet, R.; Langlet, M. *Thin Solid Films* **2000**, *372*, 177.
(18) Strohhöfer, C.; Fick, J.; Vasconcelos, H. C.; Almeida, R. M. *J. Non-Cryst. Solids* **1998**, *226*, 182.
(19) Auzel, F. E. Processes in heavily doped rare-earth materials and their application to optoelectronic devices, in *Semiconductor Optoelectronics*, Wiley: Chichester, UK, 1980; p. 233.
(20) Ghosh, N. N.; Pramanik, P. *Mater. Science Eng.* **1997**, *B49*, 79.
(21) Riello, P.; Canton, P.; Fagherazzi, G. *J. Appl. Crystallogr.* **1998**, *31*, 78.
(22) Riello, P.; Canton, P.; Comelato, N.; Polizzi, S.; Verità, M.; Fagherazzi, G.; Hofmeister, H.; Hopfe, S. *J. Non-Cryst. Solids* **2001**, *288*, 127.
(23) Ingel, R. P.; Lewis, D., III *J. Am. Ceram. Soc.* **1986**, *69*, 325.
(24) Nakagawa, K.; Izumitani, T. *J. Non-Cryst. Solids 7* **1972**, 168.
(25) Urlacher, C.; Marco de Lucas, C.; Bernstein, E.; Jacquier, B.; Mugnier, J. *Opt. Mater.* **1999**, *12*, 19.
(26) Merino, R. I.; Orera, V. M.; Cases, R.; Chamarro, M. A. *J. Phys.: Condens. Matter* **1991**, *3*, 8491.
(27) Savoini, B.; Muñoz-Santiuste, J. E.; Gonzalez, R.; Cruz, G. K.; Bonardi, C.; Carvalhao, R. A. *J. Alloys Compd.* **2001**, *323*−*324*, 748.